INVESTIGATIONS OF IRREGULARITIES IN REMOTE PLASMA REGIONS BY RADIO SOUNDING: APPLICATIONS OF THE RADIO PLASMA IMAGER ON IMAGE

SHING F. FUNG[1], ROBERT F. BENSON[1], DONALD L. CARPENTER[2], BODO W. REINISCH[3] and DENNIS L. GALLAGHER[4]
[1]*NASA Goddard Space Flight Center, Greenbelt, MD, U.S.A.*
[2]*Stanford University, Palo Alto, CA, U.S.A.*
[3]*University of Massachusetts, Lowell, MA, U.S.A.*
[4]*NASA Marshall Space Flight Center, Huntsville, AL, U.S.A.*

(Received May 7, 1999)

Abstract. The Radio Plasma Imager (RPI) on the IMAGE mission operates like a radar by transmitting and receiving coherent electromagnetic pulses. The RPI is designed to receive mirror-like (specular) reflections and coherent scatter returns. Long-range echoes of electromagnetic sounder waves are reflected at remote plasma cutoffs. Thus, analyses of RPI observations will yield the plasma parameters and distances to the remote reflection points. The RPI will employ pulse compression and spectral integration techniques, perfected in ground-based ionospheric digital sounders, in order to enhance the signal-to-noise ratio in long-range magnetospheric sounding. When plasma irregularities exist in the remote magnetospheric plasmas being probed by the sounder waves, echo signatures may become complicated. Experience in ionospheric sounding under such conditions indicates that sounding echo strengths can actually be enhanced by the presence of irregularities, and ground-based sounding indicates that coherent detection techniques can still be employed. In this paper we investigate the conditions that will allow coherent signals to be detected by the RPI and the signatures of scattering to be expected in the presence of multi-scale irregularities. Sounding of irregular plasma structures in the plasmasphere, plasmapause and magnetopause are also discussed.

1. Introduction

The Imager for Magnetopause-to-Aurora Global Exploration (IMAGE) satellite, scheduled to be launched on February 15, 2000, will carry six remote sensing instruments to study the global response of the Earth's magnetosphere to changes in the solar wind (Fuselier et al., 2000). One of the scientific instruments to be flown is the Radio Plasma Imager (RPI) which is an advanced digital radio sounder that operates like a radar. The design of the RPI is based on that of the Digisonde Portable Sounder (DPS) developed at the University of Massachusetts Lowell for ground-based observations of the ionosphere (Reinisch, 1996). By transmitting coded electromagnetic pulses, and receiving the echoes reflected from remote magnetospheric plasmas, the RPI will determine the global-scale electron density structure and dynamics of the magnetosphere.

Space Science Reviews **91:** 391–419, 2000.

1.1. RPI MEASUREMENT CAPABILITIES

The RPI operates like a radar and receives echoes of sounder waves reflected at remote plasma cutoffs. It is designed to receive mirror-like (specular) reflections and coherent scatter returns (e.g., see Sales et al., 1996). Analysis of the RPI range data is based on the assumption that the sounder waves are specularly reflected, i.e., that geometric optics holds. As a result, the echo power falls off as the inverse square of the round-trip distance traveled by the sounder signal (see Section 3.3). More details on the feasibility of detecting magnetospheric echoes by a radio sounder instrument like the RPI can be found in Calvert et al. (1995, 1997).

The RPI transmits coded electromagnetic pulses with a minimal pulse length of 3.2 ms, corresponding to a range resolution of 480 km. Transmission is accomplished by using two 500-m crossed-dipole wire antennas in the satellite spin plane. These dipoles and a 20-m dipole antenna along the satellite spin (z) axis are then used for echo reception. The three-axis dipole antenna configuration and three 300 Hz-bandwidth receivers are used for signal reception. This system allows the RPI to measure the echo signal amplitude, phase, direction of arrival, time delay, polarization and Doppler shift for each sounding measurement at frequency f (Reinisch et al., 1999, 2000). The angular resolution of direction-finding is about 1°, limited primarily by the z-antenna noise level (Calvert et al., 1995, 1997). A detailed description of the RPI instrument and analysis of the received echoes is given in Reinisch et al. (1999, 2000). In this paper, we will discuss how magnetospheric plasma waves and irregularities can affect the RPI echoes.

1.2. RADIO SOUNDING IN COLD PLASMA

Discussions of long-range sounding of magnetospheric plasmas have usually focused on the use of the so-called 'free-space', high-frequency electromagnetic waves, the ordinary (L-O) and extraordinary (R-X) modes (Stix, 1992). This type of sounding is based on the cold-plasma approximation that is valid when the phase speed of the sounder wave far exceeds the electron thermal speed of the plasma medium. Transmitted pulses in the L-O and R-X modes are reflected when they encounter their respective plasma cutoffs, $f_{\mathrm{L-O}}$ and $f_{\mathrm{R-X}}$, where the wave number $k = 0$, with

$$f_{\mathrm{L-O}} = f_{pe} \tag{1}$$

and

$$f_{\mathrm{R\text{-}X}} = \frac{f_{ce}}{2} + \tfrac{1}{2}[4f_{pe}^2 + f_{ce}^2]^{1/2}\,, \tag{2}$$

where f_{pe} and f_{ce} are the electron plasma and gyro frequencies, respectively. By displaying the apparent ranges ($ct_D/2$, where c is the speed of light and t_D is the total echo time delay) of the resulting echoes as a function of the sounding frequency f, a plasmagram is produced. The plasmagram is the magnetospheric

analog of the ionogram display produced by ionospheric sounders (Benson et al., 1998; Green et al., 2000). Using inversion techniques, the plasmagram echo traces will be converted to electron density profiles from the sounder to remote plasma regions as is done in the case of ionospheric sounding (Jackson, 1969; Huang and Reinisch, 1982). Using this sounding technique, it is feasible to obtain global-scale density structures of the magnetosphere on time scales shorter than the plasma dynamical time scales (Calvert et al., 1995, 1997; Reiff et al., 1996; Fung and Green, 1996; Green et al., 1998, 2000).

1.3. THERMAL PLASMA FFECTS

The cold-plasma approximation is valid for describing the propagation of sounder waves in most ionospheric and magnetospheric plasmas. The radio sounding technique, based on this approximation, has been successfully applied to observe the structure and dynamics of the ionosphere (Hunsucker, 1992; Jackson et al., 1980). It is important to note, however, that both ionospheric and magnetospheric plasmas have finite temperature, varying from 0.1 eV in the ionosphere to $\sim$1 keV in the outer magnetosphere. Thermal effects and plasma instabilities can lead to the generation and propagation of a variety of natural plasma waves and turbulence in ionospheric and magnetospheric plasmas (Akhiezer et al., 1975; Keskinen and Ossakow, 1983).

Although the ionosphere has usually been treated as a cold plasma, its finite temperature supports the presence of many plasma waves, such as Langmuir and ion acoustic waves (Kelley, 1989; Hargreaves, 1992). As discussed in the next section, these eigenmodes and other small-scale plasma irregularities can interact with high-frequency sounder waves to produce observable signatures in radio sounding observations. We will illustrate some examples of those signatures in Section 3.

2. Effects of Multi-Scale Irregularities on Sounder Measurements

It is generally assumed that long-range propagation of a sounder wave is supported by the background plasma such that the validity of the *WKB* approximation is maintained (Budden, 1985; Stix, 1992), i.e., that

$$\lambda \ll L_i = n_0(\nabla n_0)^{-1} , \tag{3}$$

where λ is the wavelength of the sounder wave and n_0 is the background electron density with an inhomogeneity scale length L_i. In magnetized plasmas, such as for the earth's ionosphere and magnetosphere, the approximation also requires that the variability scale length of the background magnetic field B_0 be much longer than the wavelength of the electromagnetic wave.

Due to plasma instabilities and dynamic changes, plasma irregularities and inhomogeneities are common features in ionospheric and magnetospheric plasmas.

These plasma variations, having a spectrum of spatial and temporal scales, can affect the propagation of a sounder wave, particularly at magnetospheric boundaries such as the plasmapause and magnetopause. For discussion purposes, we refer to the quasi-static variations on the largest spatial scales as L_i for the 'structures' or 'inhomogeneities' resulting from magnetospheric plasma dynamics (e.g., MHD processes). We will use λ_i to represent the wavelengths or scale sizes of irregularities associated with plasma waves or smaller scale fluctuations.

In the linear-wave approximation, perturbations (e.g., δn and δB) associated with different plasma wave modes in a plasma are too small to result in significant changes in the background density n_0 or magnetic field B_0. This approximation is considered to be well satisfied at the distant echo regions where the amplitudes of the sounder waves are small. Thus, low-amplitude sounder and naturally occurring plasma waves can be treated as independent of one another, except when they satisfy conditions for resonant interactions (see Section 2.3). The nature of the interaction between the sounder wave and a given plasma wave mode depends on the frequency f_i and wavelength λ_i of the plasma wave. When $L_i > \lambda > \lambda_i \gg \lambda_{\mathrm{De}}$ (Debye length), the plasma wave perturbations can coherently scatter the sounder wave.

Indeed, most ground-based radar observations of ionospheric irregularities result from coherent scattering (see Kelley, 1989). These observations have sometimes been labeled 'incoherent radar observations' because they have been obtained by incoherent scatter radar (ISR) facilities. Although these ISR were originally designed to observe incoherent scattering, such as Thomson scattering by individual electrons, they also detect radar echoes returned by anomalous (non-specular) reflection resulting from coherent scattering by small-scale plasma irregularities. In this paper, we will adhere to the physical definition of incoherent scattering as scattering by randomly distributed charged particles and refer to all scattering by collective plasma oscillations, such as waves and plasma irregularities, as coherent scattering.

During or shortly after periods of RPI transmission, the plasma medium in the vicinity of the spacecraft can be significantly perturbed by the transmitted wave amplitudes such that the weak turbulence (or linear) approximation is violated (Pulinets and Selegey, 1986). In this nonlinear or strong turbulence regime, significant density perturbations can be induced in the background plasma (see Section 2.4). When $\lambda > L_i$ (and λ_i), geometric optics (WKB approximation) fails and physical optics must be used to describe wave propagation. Therefore, in analyzing low-frequency sounder measurements, such as those obtained by the RPI near the low-frequency portion of a frequency sweep (while operating in remote sounding or relaxation sounding), one may have to consider the effects of multi-scale nonlinear irregularities on the sounder signals.

2.1. SIGNAL COHERENCE CONDITION

The RPI is a digital sounder designed to perform long-range sounding with low transmission power (Reinisch et al., 2000). If needed, coherent integration techniques (pulse compression and spectral integration) can be used to enhance the signal-to-noise ratios of long-range echoes (Haines, 1994; Green et al., 1998). In phase-code pulse compression, the phase code (i.e., the sequence of 0 (+) or 180 (−) degree phases of each of the multiple 3.2-ms pulse chips (see Reinisch et al., 2000) of the received echo pulse is correlated with that of the transmitted pulse. The signals are then summed coherently (by matching chip phases) to effectively enhance the signal-to-noise ratio. Hence, pulse compression depends on the preservation of the transmitted phase code in the echo pulses received by the RPI. In spectral integration, multiple pulses at the same frequency are transmitted successively and the return pulses are Fourier analyzed for each echo delay. Spectral integration is the process that combines all the Fourier components having the same Doppler shift. Signals that are in-phase will add coherently, thus enhancing the signal-to-noise ratio. The effectiveness of these signal-processing techniques depends on the degree of coherence (Hecht and Zajac, 1976) of the carrier waves that form the echo pulses.

As discussed in Reinisch et al. (1999, 2000), analysis of echo signals relies on the capability of the RPI to distinguish each echo observed. Each echo is characterized by its frequency, range, amplitude, phase, polarization, direction of arrival and Doppler shift. For the purpose of our discussion, it is important to differentiate echo signals from echo pulse. Echo signals are the electric field measurements (i.e., amplitudes and phases as a function of time and frequency) obtained by the three RPI receivers. An echo pulse or chip comprises a narrow spectrum of Fourier components, centered on a central frequency. Phase code coherence of pulses refers then to the matching of the bi-phases (+ or −) of the chips within the pulses. On the other hand, signal coherence, described in Section 2.1.1 below, pertains to the phase relationship between the carrier waves that form the pulses. Thus, before considering further the effects of multi-scale plasma fluctuations on a sounder wave, it is important to determine the conditions under which pulse integrity and echo coherence are maintained so that coherent integration can be used. One way to do so is to consider the coherence of all the signals within a given echo received by the three orthogonal RPI antennas, defined simply as all the signals falling within one range bin Δr and one Doppler bin ΔD (in frequency) for a given sounding frequency.

2.1.1. *Signal coherence*

When probing a quasi-static remote plasma region at a range $\mathbf{r}$ ($= r\hat{\mathbf{r}}$) with a sounder wave of a given frequency f, all the signals reflected by the distant reflecting surface will interfere constructively or destructively among the returning waves to varying degrees, depending on the phase path differences (PPD). Two wave

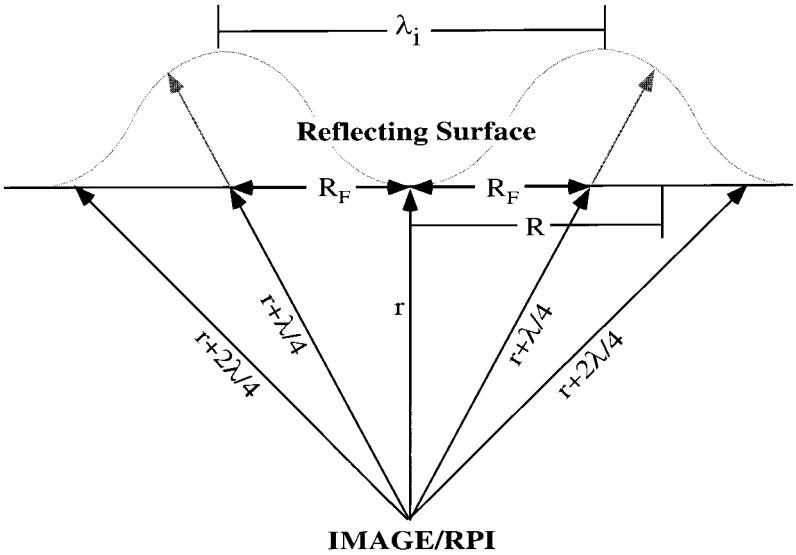

Figure 1. Sounder wave trains are in-phase when their reflection points are located within the primary Fresnel zone with a diameter $2R_F$ ($m = 1$), resulting in strong, coherent signals. The addition of signals from external regions (e.g., $m = 2$) will diminish the received echo signal. The solid-horizontal line and the light gray-wavy line represents schematically a planar and a rough reflecting surface, respectively.

trains are considered to be operationally 'in phase' and will interfere constructively when the total PPD between them is $< \lambda/4$. They are coherent when the PPD is constant (Hecht and Zajac, 1976). If the PPD of the wave trains relative to one another varies slowly with time, the time interval over which the constancy of the relative phase difference is maintained is known as the coherence time. Coherent signals reflected by a quasi-static plasma surface have a coherence time given by the dynamical time scale of the reflecting surface.

Figure 1 shows a schematic of the coherent waves at a given frequency f returning from within an annular region of radius R in a static planar reflecting surface in the target region, such that r, R, and λ satisfy the condition

$$(r^2 + R^2) \leq \left(r + m\frac{\lambda}{4}\right)^2 . \tag{4}$$

All the signals returning from within the regions of $m = 1, 3, 5, \ldots$, etc. will be in-phase and coherent with the wave returning along $\mathbf{r}$ ($R = 0$ and $m = 0$) and thus will add to the signal strength. Signals reflected near R with $m = 2, 4, 6, \ldots$, etc. will be completely out of phase (but also coherent) with the signals along $\mathbf{r}$ and thus will attenuate the signal. For the case of $r \gg \lambda$ and $m = 1$, (4) leads to the definition of the Fresnel radius R_F in optics,

$$R_F = \sqrt{r\lambda/2} . \tag{5}$$

Although the out-of-phase signals (with net effective PPD $> \lambda/4$) will in principle interfere destructively, variations of target range and velocity due to the presence of plasma irregularities (see the light-gray portion of Figure 1 and Section 2.1.3) will result in phase randomization of the waves rather than complete cancellation of signals. For simplicity, we will neglect from here on the higher order Fresnel regions ($m > 2$) in our discussion because, at least in the plane reflecting surface approximation (see Figure 1), the signals from those regions will be oblique to the surface normal and will not likely return to the RPI.

In the presence of plasma irregularities, density fluctuations normal to the average surface of reflection at $\mathbf{r}$ can introduce an undetermined amount of additional phase path lengths to each reflected wave, causing phase mixing of the reflected waves (light-gray portion in Figure 1). This effect would be minimized when the irregular density surfaces being probed by the sounder signals satisfy the planar condition:

$$\lambda < \left(\frac{1}{n}\frac{\partial n}{\partial r}\right)^{-1} \ll \left(\frac{1}{n}\frac{\partial n}{\partial \zeta}\right)^{-1} \tag{6}$$

in which $n = n_0 + \delta n$ is the total electron plasma density and $\partial n/\partial r$ and $\partial n/\partial \zeta$ are the derivatives of the electron density perpendicular to and in the reflecting surface, respectively (see Figure 1). Thus, we can regard all the signals returned from within the primary Fresnel zone ($m = 1$) of diameter $2R_F[= \sqrt{(2\lambda r)}]$ at the reflection surface as coherent and in-phase. When there exist plasma fluctuations with $\lambda_i < \lambda < R_F$, however, the fluctuations can scatter the sounder wave. The coherence of the combined signals from multiple Fresnel zones (e.g., from $m = 1$ and $m = 2$ regions) can be degraded when plasma fluctuations are present over a broad region in the target plasma. Table I provides some examples of Fresnel zone sizes ($2R_F$) for different sounding frequencies and ranges. The comparison between the first and fourth columns in Table I, appropriate for magnetopause and ionospheric sounding, respectively, indicates quite similar sounding conditions ($2R_F/\lambda \sim 100$) for the two cases. Echo power considerations are given in Calvert et al. (1995) and in Section 3.3.

2.1.2. *Doppler shift*

In order to determine the conditions for echo coherence, one needs to consider all signals within one range bin Δr and one Doppler bin ΔD for a given sounding frequency. The Doppler shift Δf caused by the relative motion (along the range vector $\mathbf{r} = r\hat{\mathbf{r}}$) between any given target plasma moving at $\mathbf{V}_p$ (reflection point $\mathbf{P}$ in Figure 2) and the IMAGE spacecraft at $\mathbf{V}_{s/c}$ is simply given by:

$$\frac{\Delta f_P}{f} = \frac{2(\mathbf{V}_P - \mathbf{V}_{s/c}) \cdot \hat{\mathbf{r}}_P}{c} . \tag{7}$$

The factor of 2 accounts for the fact that the sounder wave has traversed the range between the sounder and the target region twice, once in each direction (e.g., see

TABLE I

Sample Fresnel zone sizes for different frequencies and ranges appropriate for magnetospheric and ionospheric sounding

	30 kHz	300 kHz	1 MHz	3MHz
λ	10 km	1 km	0.3 km	0.1km
r	4 R_E	2 R_E	4 R_E	0.1 R_E
$2R_F$	714 km	160 km	124 km	11 km

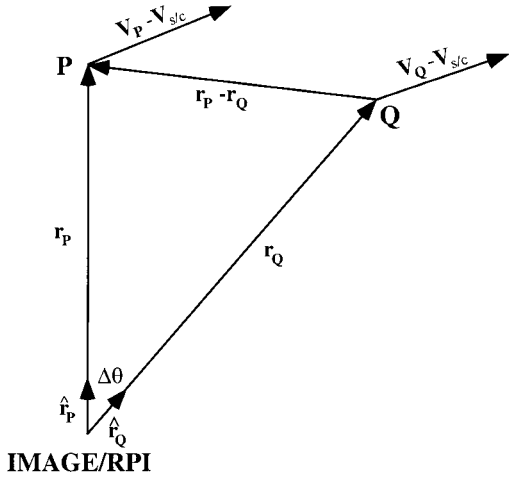

Figure 2. Schematic of two signals separated by an angular distance $\Delta\theta$ with slightly different Doppler shifts.

Bibl and Reinisch, 1978; Flock, 1979). If there are structures or irregularities in the remote plasma region such that there is another reflection point **Q** located near **P** (see Figure 1), say at an angular distance $\Delta\theta$ (as illustrated in Figure 2), its signals will have a Doppler shift Δf_Q, given by

$$\frac{\Delta f_Q}{f} = \frac{2(\mathbf{V}_Q - \mathbf{V}_{s/c}) \cdot \hat{\mathbf{r}}_Q}{c} \,. \tag{8}$$

Since the sounder wave frequency is usually much higher than the plasma frequency of the medium over large distances in the magnetospheric cavity except near the reflection point (Green et al., 2000), we can adopt straight-line propagation of the sounder wave for the present discussion. From (7) and (8) we obtain the difference in Doppler shifts between the two signals as

$$\Delta f_P - \Delta f_Q = \frac{2f}{c}[(\mathbf{V}_P - \mathbf{V}_{s/c}) \cdot \hat{\mathbf{r}}_P - (\mathbf{V}_Q - \mathbf{V}_{s/c}) \cdot \hat{\mathbf{r}}_Q] \,. \tag{9a}$$

Thus two signals, as shown in Figure 2, will contribute to the same echo observed by the RPI when they fall within a given Doppler bin ΔD, or with $\Delta\mathbf{V} = \mathbf{V}_P - \mathbf{V}_Q$,

$$\frac{2f}{c}[(\mathbf{V}_P - \mathbf{V}_{s/c}) \cdot \hat{r}_P - (\mathbf{V}_P - \mathbf{V}_{s/c}) \cdot \hat{r}_Q + \Delta\mathbf{V} \cdot \hat{r}_Q] \leq \Delta D \ , \tag{9b}$$

When $\mathbf{Q}$ is close to $\mathbf{P}$, so that $\Delta\mathbf{V}$ is small compared to $(\mathbf{V}_P - \mathbf{V}_{s/c})$, then (9b) becomes

$$\frac{2f}{c}[(\mathbf{V}_P - \mathbf{V}_{s/c}) \cdot (\hat{\mathbf{r}}_P - \hat{\mathbf{r}}_Q)] \leq \Delta D \ , \tag{10a}$$

or, for $\Delta\theta \ll 1$ and $|\hat{\mathbf{r}}_P - \hat{\mathbf{r}}_Q| = \Delta\theta$, we have

$$\frac{2f\,\Delta\theta|\mathbf{V}_P - \mathbf{V}_{s/c}|\cos\,\alpha}{c} \leq \Delta D \ , \tag{10b}$$

where α is the angle between $(\mathbf{V}_P - \mathbf{V}_{s/c})$ and $(\hat{\mathbf{r}}_P - \hat{\mathbf{r}}_Q)$. Thus, for a given Doppler bin ΔD and a plasma velocity $\mathbf{V}_p$, the condition in (10b) provides the limiting angular width of an area in the remote target plasma region from which all the signals contributing to an RPI measured echo are reflected (Bibl and Reinisch, 1978).

2.1.3. *Coherence Condition*

In this subsection, we determine the conditions under which two signals arriving within a solid angle of width $\Delta\theta$ are coherent. To that end, we consider two coherently transmitted wave trains after total specular reflection at their reflection points. Without loss of generality, we only need to consider one component of the electric field vectors:

$$E_1 = E_{01}\sin(\omega t - \mathbf{k}_1 \cdot \mathbf{r}_1 + \varepsilon) \ , \tag{11}$$

$$E_2 = E_{02}\sin(\omega t - \mathbf{k}_2 \cdot \mathbf{r}_2) \ , \tag{12}$$

with ε being a constant phase difference between E_1 and E_2. If both E_1 and E_2 returned to the RPI within the same range bin and Doppler bin, then they both would contribute to the same echo signal E, such that $E = E_1 + E_2$, or

$$E = E_{01}\sin(\omega t - \mathbf{k}_1 \cdot \mathbf{r}_1 + \varepsilon) + E_{02}\sin(\omega t - \mathbf{k}_2 \cdot \mathbf{r}_2) \ . \tag{13}$$

Since E_1 and E_2 were transmitted simultaneously and received within one range bin (i.e., nearly simultaneously), we have $E_{01} = E_{02} = E_0$ so that (13) becomes

$$\begin{aligned} E \ &= E_0[\sin(\omega t - \mathbf{k}_1 \cdot \mathbf{r}_1 + \varepsilon) + \sin(\omega t - \mathbf{k}_2 \cdot \mathbf{r}_2)] \\ &= 2E_0\cos\left(\frac{\mathbf{k}_1 \cdot \mathbf{r}_1 - \varepsilon - \mathbf{k}_2 \cdot \mathbf{r}_2}{2}\right)\sin\left[\omega t - \left(\frac{\mathbf{k}_1 \cdot \mathbf{r}_1 - \varepsilon + \mathbf{k}_2 \cdot \mathbf{r}_2}{2}\right)\right] \ . \end{aligned}$$

Now, let $\mathbf{k}_2 = \mathbf{k}_1 + \Delta\mathbf{k}$ and $\mathbf{r}_2 = \mathbf{r}_1 + \Delta\mathbf{r}$ then E can be rewritten as

$$E = 2E_0 \cos\varphi \sin(\omega t - \mathbf{k}_1 \cdot \mathbf{r}_1 + \varepsilon - \varphi)$$

where we have defined

$$\varphi = \frac{\varepsilon + \mathbf{k}_1 \cdot \Delta\mathbf{r} + \Delta\mathbf{k} \cdot (\mathbf{r}_1 + \Delta\mathbf{r})}{2} .$$

It is clear then that when there exist fluctuations or irregularities in the remote plasma regions, phase variations ($\Delta\mathbf{k}$, $\Delta\mathbf{r}$) can be introduced to the signals returned within a given Doppler bin and range bin relative to the original transmitted waves. The resultant amplitude is also modulated by the $\cos\varphi$ factor. In order for the reflected signals to remain coherent (and in phase) with the transmitted wave, we require that $\varphi - \varepsilon/2 = \pi/8$ (i.e., a total round-trip phase difference of $\pi/4$)

$$\frac{\mathbf{k}_1 \cdot \Delta\mathbf{r} + \Delta\mathbf{k} \cdot (\mathbf{r}_1 + \Delta\mathbf{r})}{2} \leq \frac{\pi}{8} . \tag{14}$$

For $\Delta\mathbf{r} = \mathbf{r}_2 - \mathbf{r}_1$ and $\Delta\mathbf{k} = \mathbf{k}_2 - \mathbf{k}_1$ we can write $|\mathbf{r}_2| = |\mathbf{r}_1| \pm \delta r$ with δr being the range variations ($\pm$) within a range bin (480 km for a 3.2 ms pulse) and $|\mathbf{k}_2| = |\mathbf{k}_1| + \delta k$ with δk being the variation in Doppler shifts among the signals. The latter condition is determined from the fact that both k_1 and k_2 have been Doppler shifted from k_0, the transmitted wave number, upon reflection at their respective reflection points. We thus have

$$\mathbf{k}_1 \cdot \Delta\mathbf{r} + \Delta\mathbf{k} \cdot (\mathbf{r}_1 + \Delta\mathbf{r}) = -k_1 r_1 + k_2 r_2 = r_1 \delta k \pm k_1 \delta r ,$$

and the coherence condition (14) becomes

$$\frac{r_1 \delta k \pm k_1 \delta r}{2} \leq \frac{\pi}{8} . \tag{15}$$

The second term on the left-hand side is simply the Rayleigh criterion for surface roughness. If we now focus on the first term only (by letting $\delta r = 0$), then

$$r_1 \delta k \leq \frac{\pi}{8} . \tag{16}$$

Since $\delta k = (2\pi \Delta D)/c$, substituting (10b) for the limit of small plasma velocity gradients into (16) then yields

$$\frac{4\pi r_1 f \Delta\theta |\mathbf{V}_P - \mathbf{V}_{s/c}| \cos\alpha}{c^2} \leq \frac{\pi}{4}$$

or,

$$r_1 \leq \frac{\lambda c}{16 \Delta\theta |\mathbf{V}_P - \mathbf{V}_{s/c}| \cos\alpha} \equiv r_c . \tag{17}$$

TABLE II

Representative values of Debye length for different regions in the magnetosphere

Region	Nominal n_0, T	λ_{De}
Magnetospheric lobe or cavity	$n_0 \sim 0.1$ cm^{-3}, $T < 1$ keV	<743 m
Magnetopause boundary	$n_0 \sim 1$ cm^{-3}, $T < 1$ keV	<235 m
Within the plasmapause	$n_0 > 10^3$ cm^{-3}, $T < 1$ eV	<0.25 m

2.2. ORDERING OF SCALE SIZES

It is apparent that the echo characteristics to be received by the RPI are determined by the various characteristic scale sizes mentioned. Within the limits of (3) and (6), we need to consider the ordering of λ, λ_i, λ_{De}, and R_F for a given sounding observation from a range r and sounder frequency setting. The RPI operates in the frequency range 3 kHz $\leq f \leq$ 3 MHz, thus the corresponding wavelength range is $0.1 \leq \lambda \leq 100$ km (see Table I above). Since the electron density and temperature encountered by an RPI transmitted wave range between $0.1–10^5$ cm^{-3} and 10^{-3}–1 keV, respectively, the typical Debye lengths are given in Table II.

For linearly propagating sounder waves that satisfy (3) and (6), the parameters provided in Tables I and II indicate that the sounder wave can encounter a full range of plasma irregularity scale sizes given by $L_i > R_{\mathrm{F}} > (\lambda >$ or $< \lambda_i) \gg \lambda_{\mathrm{De}}$. When $\lambda < \lambda_i$, the sounder wave will simply behave as if it is traversing a medium with large-scale irregularities L_i under the *WKB* approximation. Calvert et al. (1995) have in fact investigated the effects of large-scale irregularities on the sounder signals and determine the focusing and de-focusing of the echo signals associated with concave and convex reflectors, respectively. On the other hand, when $\lambda > \lambda_i$, the sounder wave can be coherently scattered by plasma waves.

2.3. COHERENT SCATTERING OF SOUNDER WAVE

Scattering refers to the interaction of a transmitted wave with a scattering center that is small compared to the wavelength (i.e., $\lambda_i < \lambda \ll L_i$), such that after the interaction the scattered wave propagates into a direction different from that of the transmitted wave. Incoherent scattering occurs when $\lambda < \lambda_{\mathrm{De}}$ so that individual charged particles act as scattering centers. Due to the low transmitter power of the RPI, incoherent scattering is not a significant effect to be considered. Coherent scattering occurs when $\lambda \geq \lambda_i \gg \lambda_{\mathrm{De}}$ such that the scattering centers are provided by the collective action of the perturbations in a plasma, such as those associated with plasma waves. Coherent scattering can lead to backscattering, or aspect-sensitive scattering of sounder signals, leading for example to the observations of field-

aligned irregularities in the ionosphere (see Sections 2.3.2 and 3.1). In long-range sounding, the backscattered signals may be too weak for detection. Having suffered coherent scattering, however, the echo power can also be significantly degraded. Thus, it is pertinent to study the coherent scattering processes that may affect the quality of the RPI signals.

2.3.1. *Raman and Brillouin Scattering*

The most common processes by which high-frequency electromagnetic waves are scattered by a plasma are the stimulated Raman and Brillouin scattering (Kruer, 1988; Swanson, 1989). These processes are quite similar in that they are both three-wave processes involving an incident electromagnetic wave (ω_0, $\mathbf{k}_0$), a scattered electromagnetic wave (ω_s, $\mathbf{k}_s$), and a plasma wave (ω_i, $\mathbf{k}_i$). In Raman scattering, the plasma wave is a Langmuir wave; whereas in Brillouin scattering, the corresponding plasma wave is an ion acoustic wave.

The scattering processes can be generally described by the weakly-nonlinear plasma theory (Davidson, 1972; Fejer and Kelley, 1980) as a three-wave decay process in which the following wave resonance conditions are satisfied (conventionally expressed in terms of the wave angular frequencies ω and wave vectors $\mathbf{k}$):

$$\mathbf{k}_0 = \mathbf{k}_s + \mathbf{k}_i \tag{18}$$

and

$$\omega_0 = \omega_s + \omega_i \ . \tag{19}$$

As the sounder wave encounters a plasma medium in which plasma waves are present, it can be scattered by the plasma wave when (18) and (19) are locally satisfied.

The physics of the scattering process is fairly straightforward. When the high-frequency wave propagates through a plasma medium, its oscillating electric field with amplitude E_0 may encounter rippling density perturbations associated with a plasma wave along its propagation path. In responding to the incoming wave field, the plasma electrons will oscillate with a velocity $v = eE_0/m\omega_0$, which in turn generates a transverse current $\delta J = -ev\delta n$. When the phase-matching conditions (18) and (19) are satisfied, the transverse current can then generate the scattered wave field. It can be shown that the scattering cross section maximizes for the case of backscattering of unpolarized waves (Akhiezer et al., 1975).

For backscattering, we have $\mathbf{k}_s = -\mathbf{k}_0$ such that (18) implies that $k_i = 2k_0$. This is a general result pertaining to backscattering from irregularities or plasma waves. In the case of Raman scattering, since ω_i of a Langmuir wave is near the local plasma frequency ω_{pe}, and the scattered wave frequency is $\omega_s \geq \omega_{pe}$, therefore we must have $\omega_0 \geq 2\omega_{pe}$. This implies that Raman backscattering would occur at a density near $n_{cr}/4$, where n_{cr} is the critical electron density defined by the *L-O* mode cutoff [(1)] of the transmitted wave (ω_0, $\mathbf{k}_0$). Within the limit $(k_i\lambda_{\mathrm{De}})^2 \ll 1$,

Brillouin (and Raman) backscattering causes the returned signals to be shifted in frequency ($\omega_s = \omega_0 - \omega_i$). Since the ion-acoustic wave frequency is given by $\omega_i = k_i\sqrt{(T_e/M_i)} \approx 6.15 \times 10^4\sqrt{(T_e/\lambda_i^2)}$ rad s^{-1}, where T_e is the electron temperature in electron-volts and λ_i is the wavelength in meters, we can estimate the frequency shift as $\Delta f = \omega_i/2\pi$. Using the backscattering condition $\lambda_i \approx \lambda/2$, we thus have $\Delta f/\sqrt{(T_e)} = 2$, 20 and 65 Hz eV$^{-1/2}$ for the sounder wave frequency of 30 kHz, 300 kHz, and 1 MHz, respectively. The actual frequency shifts, dependent on the electron plasma temperature, can be measured by the Doppler shift measurements (Reinisch et al., 1999, 2000).

2.3.2. *Aspect-Sensitive Scattering*

As discussed in Section 3.1 below, the ionospheric spread-F phenomenon is the result of scattering of radio sounder signals by ionospheric field-aligned irregularities (FAI). High-frequency electromagnetic waves propagating nearly transversely with respect to the background magnetic field can be scattered by the FAI. A coherent condition selects scattering from irregularities whose spacing equals half the sounder wavelength (Hanuise, 1983; James, 1989). This condition is simply the backscattering condition ($k_i = 2k_0$) discussed in the last sub-section. Detailed descriptions of the theory and observations of aspect-sensitive scattering in the ionosphere can be found in Fejer and Kelley (1980) and Hanuise (1983). A recent application of a digital ionosonde to observe ionospheric FAI is given in Sales et al. (1996).

2.4. STRONG TURBULENCE PROCESSES

We have so far treated all wave modes and the plasma medium to be well described by the linear or weak turbulence theory (Davidson, 1972). In fact, when the wave energy (W) becomes comparable to the plasma thermal energy ($W_{th} = nT_e$), the plasma medium in which the waves propagate can become a nonlinear medium, such that the dielectric tensor becomes a function of the wave amplitudes. In this case, perturbation techniques no longer provide adequate descriptions of the wave-plasma interactions (see e.g., Treumann and Baumjohann, 1997). When $W/W_{th} > 1$, the plasma medium is significantly modified by the presence of waves near the spacecraft (Pulinets and Selegey, 1989) or in remote plasma regions where plasma instabilities can lead to significant wave levels (e.g., Anderson et al., 1982; Gary and Sgro, 1990; Drake et al., 1994). Strong plasma turbulence effects become important when $W/W_{th} > (k_i\lambda_{\mathrm{De}})^2$. Density variations, such as density depletions known as cavitons, associated with strong ion-acoustic and Langmuir turbulence may be involved in the formation of density striations in the auroral and equatorial upper ionospheres (Treumann and Baumjohann, 1997). These strong density perturbations can affect the propagation of the sounder signals. Detailed treatment of strong plasma turbulence is beyond the scope of this paper. Suffice it to note, however, that the effects of strong plasma turbulence, if present in remote

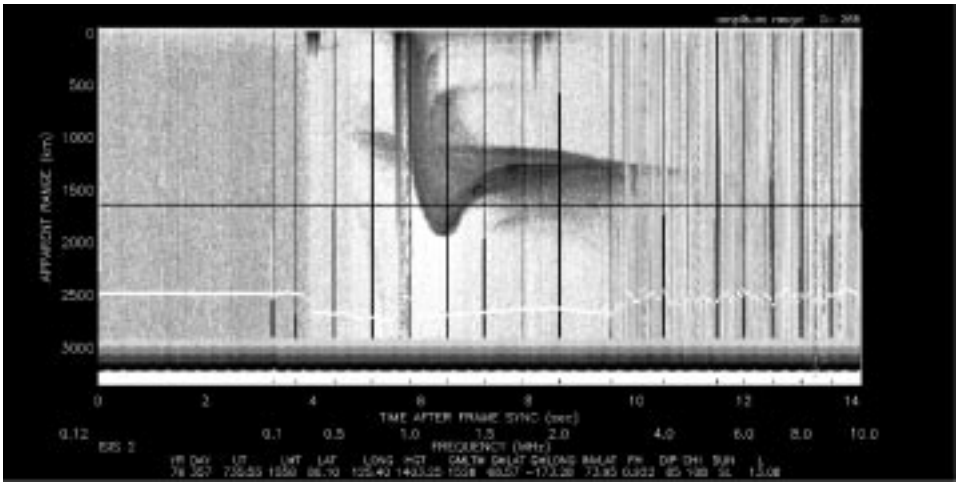

Figure 3. Digital ISIS-II high latitude ionogram recorded at the Resolute Bay telemetry station on day 357 of 1976 at 07:35:50 UT. (Digital ISIS data are available from the National Space Science Data Center at http://nssdc.gsfc.nasa.gov/space/isis/isis-status.html.)

target plasma regions, can be manifested in the RPI signals, particularly from the ionosphere and plasmasphere where the thermal plasma energy densities are low, and from the cusp and magnetopause regions where plasma turbulence is prevalent.

3. Detection of Remote Ionospheric Irregularities by Space-Borne Radio Sounders

In the terrestrial ionosphere and magnetosphere, irregularities in electron density sometimes form in the direction perpendicular to the ambient magnetic field **B**. These density irregularities are referred to as field-aligned irregularities (FAI) because they are usually maintained for long distances along **B**. FAI are easily detected by observing the radio waves that are either scattered by them or are guided (ducted) along them. The most common ionospheric signature of FAI is in the form of spread F, i.e., the spreading in both range and frequency of the F region reflection traces on ionograms from both ground-based and satellite-based ionosondes. Topside ionograms from the latter also display spectacular signatures of ducted echoes resulting from radio waves guided along FAI. We review in this section some signatures of ionospheric plasma irregularities observed in topside ionograms, which can serve as a guide to the analogous magnetospheric observations by the RPI.

3.1. SPREAD F

Ionogram spread-F signatures are attributed to aspect-sensitive scattering (see Subsection 2.3.2) from FAI with irregularity scale sizes transverse to **B** equal to one

half of the wavelength of the probing sounder wave (e.g., Fejer and Kelley, 1980; James, 1989). The scattered signal often has an intensity equal to or greater than the signal from the totally reflected wave as illustrated by the ISIS 2 observations shown in Figure 3, which also illustrates that the spread-F can extend over a great altitude range. In this example, the spread-F signature extends from the altitude of the electron density F-peak to the altitude of the spacecraft. The spread F provides valuable information concerning the presence and nature of FAI, but can greatly complicate the inversion of ISIS 2 ionograms to produce electron density profiles (Hagg et al., 1969). This ionogram also displays whistler-mode noise during the fixed-frequency portion of sounding operations (in this case, at 0.12 MHz for about the first 3.3 s of the ionogram) and continuing into the swept-frequency operation until the local plasma frequency is encountered near 0.37 MHz. In addition, noise signals from the ionospheric breakthrough of ground-based radio transmitters are observed at frequencies above about 3.0 MHz.

3.2. DUCTED ECHOES

When a topside sounder is immersed in a FAI that extends from one hemisphere to the other, long-range non-vertical echoes (Muldrew, 1969; Calvert, 1995) can be received as schematically illustrated in the top half of Figure 4. In this schematic, a satellite-borne sounder immersed in a FAI associated with an equatorial plasma bubble is illustrated with ray paths of expected ionospheric echoes. The expected ionogram traces produced by these echoes are illustrated in the schematic ionogram inserts adjacent to each reflection point. The ionogram insert for trace #1 corresponds to the radio waves that travel the shortest distance to their total reflection directly below the satellite, i.e., to vertical propagation in a horizontally stratified ionosphere. The ionogram insert for trace #2 corresponds to propagation along the FAI in the local hemisphere. This trace is of longer duration than trace #1 because the waves along the non-vertical path have a longer distance to travel to encounter the same n_0 value compared to the vertically-propagating waves in a horizontally stratified ionosphere. Note that the FAI depicted in the figure only needs to correspond to a $\delta n/n_0$ of a few percent to give rise to ducted echoes (Dyson and Benson, 1978).

The ionogram insert for trace #3 is of much greater duration and has a different shape. It corresponds to reflections of the ducted waves in the conjugate hemisphere. In this case, the first signal return (corresponding to the wave cutoff frequency) occurs at a finite delay time because no echo is returned from the regions of lower n_0 above the satellite along this ducted propagation path into the conjugate hemisphere. This first signal return corresponds to the location in the conjugate hemisphere where n_0 is the same as the value corresponding to the wave cutoff conditions [(1) or (2)] at the satellite location. The delay (for trace 3) then decreases with increasing frequency above wave cutoff due to decreasing wave retardation with increasing frequency. The ionogram insert for combinations of

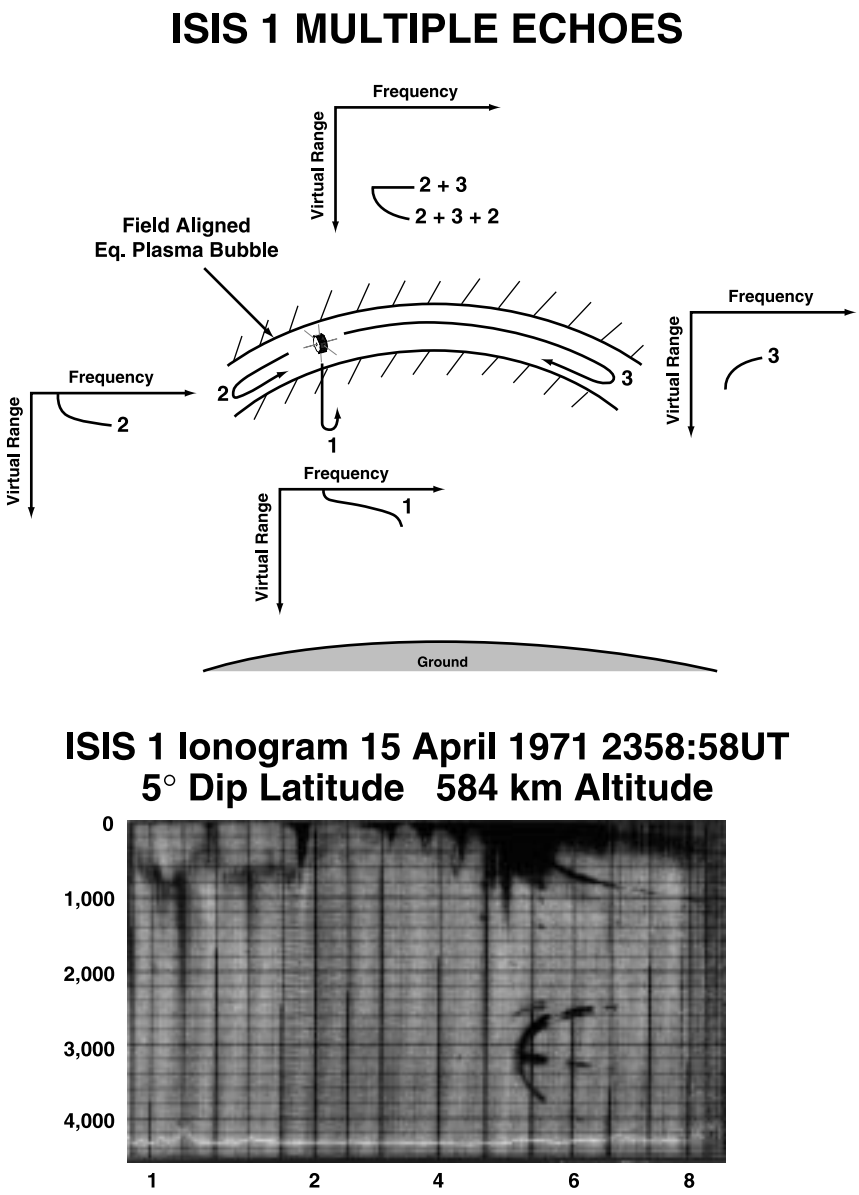

Figure 4. Schematic and ISIS 1 observations of equatorial-bubble duct (adapted from Dyson and Benson, 1978).

these ducted echoes is shown at the very top of Figure 4. Combining these multiple echoes with trace #3 (right schematic insert) yields an epsilon signature exactly as observed in the low-latitude, low-altitude ISIS 1 ionogram reproduced in the lower portion of Figure 4.

3.3. EFFECTS OF PLASMA IRREGULARITIES ON SIGNAL STRENGTHS OF LONG-RANGE ECHOES

Next we will consider the effect of plasma irregularities in the reflecting medium on the signal strength of long-range echoes that are anticipated in magnetospheric sounding. First, it is important to emphasize that in radio sounding, which has been performed in the ionosphere for decades and will be performed in the magnetosphere by RPI on IMAGE, the received echo power is proportional to the inverse square of the total round-trip path length involved. This dependence on the inverse square of the distance is appropriate because the sounder signals are returned by a specular reflection process [e.g., see the discussions in Ratcliffe (1970, Chapter 2; 1972; Chapter 9). This is different from the situation of isotropic scattering from a small target in which the returned power falls off as the inverse fourth power of the range (for example, see Tyler et al., 1992). When the target is distributed relative to the antenna beam, the inclusion of the total scattering volume also leads to an r^{-2} dependence (e.g., see Flock, 1979, Chapter 6). In this regard, it is important to note that even though the RPI antenna pattern is very broad (much broader than the target), the returning signals due to total reflection (rather than back scatter) will have an r^{-2}-dependence.

As discussed in the above subsections, space-borne radio sounders can detect prominent scatter signal returns from FAI. Our concern here is on the effect such irregularities will have on the reception of long-range echoes. Experience gained from three decades of topside-sounding of the ionosphere provides some degree of confidence that magnetospheric echoes will be observable. An obvious difference between ionospheric and magnetospheric sounding, however, is that distances are shorter and the operating frequencies are higher (where the space-borne antennas are more efficient) in the case of ionospheric sounding. A particular issue, as discussed by Calvert et al. (1995) and Benson et al. (1998), is sounding the low density magnetopause which requires the detection of long-range echoes at frequencies as low as 30 kHz. Considering low-frequency sounding at such distances (about 2 R_E from the IMAGE apogee radial distance of 8 R_E) based on ionospheric-sounding experience, Benson et al. (1998) pointed out 9 advantages that RPI will have over the ISIS-type experiment for the detection of long-range echoes. These ranged from a 3 dB gain from using two transmitters to drive the two spin-plane dipoles $\pm 90°$ out of phase in order to transmit R-X or L-O waves (ISIS used one transmitter into one of two crossed dipoles), to a 22 dB gain from an increased S/N ratio due to a smaller receiver bandwidth (300 Hz compared with 50 kHz on ISIS). Details of the RPI capabilities, including transmission efficiency as a function of frequency and coherent integration techniques, for performing radio sounding of the magnetosphere have been provided in Reinisch et al. (2000).

Franklin and Maclean, (1969, p. 904) and Jelly and Petrie (1969) presented results from investigations of the effect of plasma irregularities in the reflecting medium on the received echo signal strength in the case of ionospheric sounding

from the Alouette 1 & 2 satellites. They compared the observed signal strength to that expected from a mirror reflection assuming an inverse square power fall off with the round-trip distance (as discussed above). They found that there was an increase of up to 10 dB in the signal level, on ionograms recorded in the presence of spread F, to that expected assuming a mirror reflection. Such results indicate that irregularities in the reflecting region may actually increase the power returning to the sounder by allowing more rays (from the broad antenna pattern) to satisfy the conditions of total reflection. Similar circumstances may be true in the case of magnetospheric sounding as irregularities are also common occurrences in magnetospheric plasmas.

4. Observing Magnetospheric Plasma Irregularities

In this section, we consider in some detail the remote sensing of irregular structures in the plasmasphere and plasmapause and briefly consider observing the large-scale variations in the magnetopause boundary layer region.

4.1. PLASMASPHERE AND PLASMAPAUSE

In situ observations by a number of satellites, particularly by ISEE 1 and more recently CRRES during passages through the equatorial plasmasphere, have revealed remarkable variability and plasma irregularities near the plasmapause and within outlying regions (e.g., Oya and Ono, 1987; Koons, 1989; Horwitz et al., 1990; Carpenter et al., 1993; LeDocq et al., 1994; Moldwin et al., 1995). The irregularities at or near the plasmasphere surface may appear at essentially any local time. Although the conditions under which irregular density structure develops in the region of plasmapause density gradients and in the outer plasmasphere are still unknown (Lemaire and Gringauz, 1998), their interpretation and that of many *other* phenomena studied remotely will be enhanced by the ability of IMAGE to make local measurements along its orbit as it approaches or penetrates the plasmasphere boundary (Reinisch et al., 2000; Green et al., 2000; Carpenter and Lemaire, 1997).

Figure 5 shows a near-equatorial density profile along an ISEE 1 orbit in the afternoon sector. The position of the satellite in geocentric distance as a function of MLT is shown in the inset. The profile shows irregular structure at the plasmapause ($L \sim 3.5$), an only slightly structured outlier near $L = 6$, and a patchy, irregular region of dense plasma beyond $L = 7$. The plasma frequencies corresponding to the density scale on the left are shown at the right. This is the likely density setting in which the RPI will operate in the early mission phase of IMAGE. The densities involved in off-equatorial probing by RPI may be somewhat larger, but probably not much more than a factor of $\sim$2 above those indicated.

As an example of the rapid density change in a given local time sector, Figure 6 shows two plots of electron densities measured along two consecutive CRRES

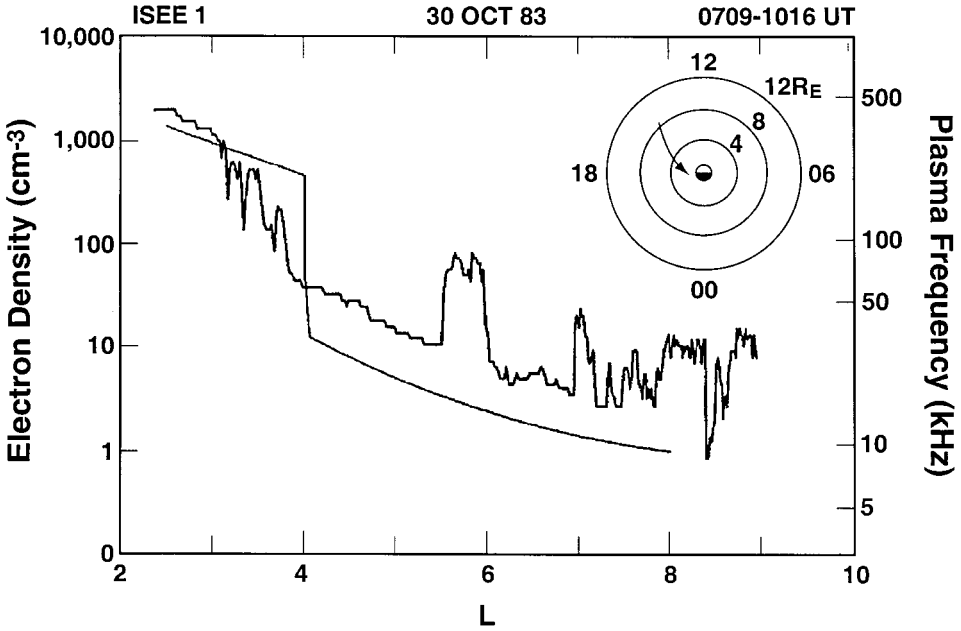

Figure 5. A near-equatorial density profile along an ISEE 1 orbit in the afternoon sector (adapted from Carpenter et al., 1993).

orbits near the equator in the post-midnight/morning sector, showing how much the plasmasphere structure can change within 10 hours during a calm period. Orbits 145 (panel A) and 146 (panel B) occurred in succession during a period of quieting following an earlier episode of plasmasphere erosion. Logarithmic n_0 is plotted vertically from the magnetic equatorial plane in coordinates of satellite L value as a function of MLT. The two curves mark the expected density levels of the quiet plasmasphere (upper curve) and the nighttime plasmatrough (lower curve) region according to an empirical model (Carpenter and Anderson, 1992). During orbit 145, the form of the density distribution was very simple, with a well-defined plasmapause and well-behaved profiles within the plasmasphere and in the trough region. However, during orbit 146, dense plasma extended farther in L value and in general the profiles were highly structured. Local density troughs appeared both inbound and outbound in the $L = 3{-}4$ range. Much of what was seen on orbit 146 may be attributed to density structure imposed in an earlier MLT sector and transported into the MLT sector of the CRRES orbit by the effects of the Earth's corotation electric field. Recall that CRRES was in a low-inclination orbit (usually with magnetic latitude $<30°$), and moved quasi-synchronously with the Earth, while IMAGE, in a high-inclination orbit, might be expected to see how a change such as that from 145 to 146 occurs at a given meridian as the 'changes' rotate into 'view.' (From EUV near apogee, a global perspective on the changes should be obtained.)

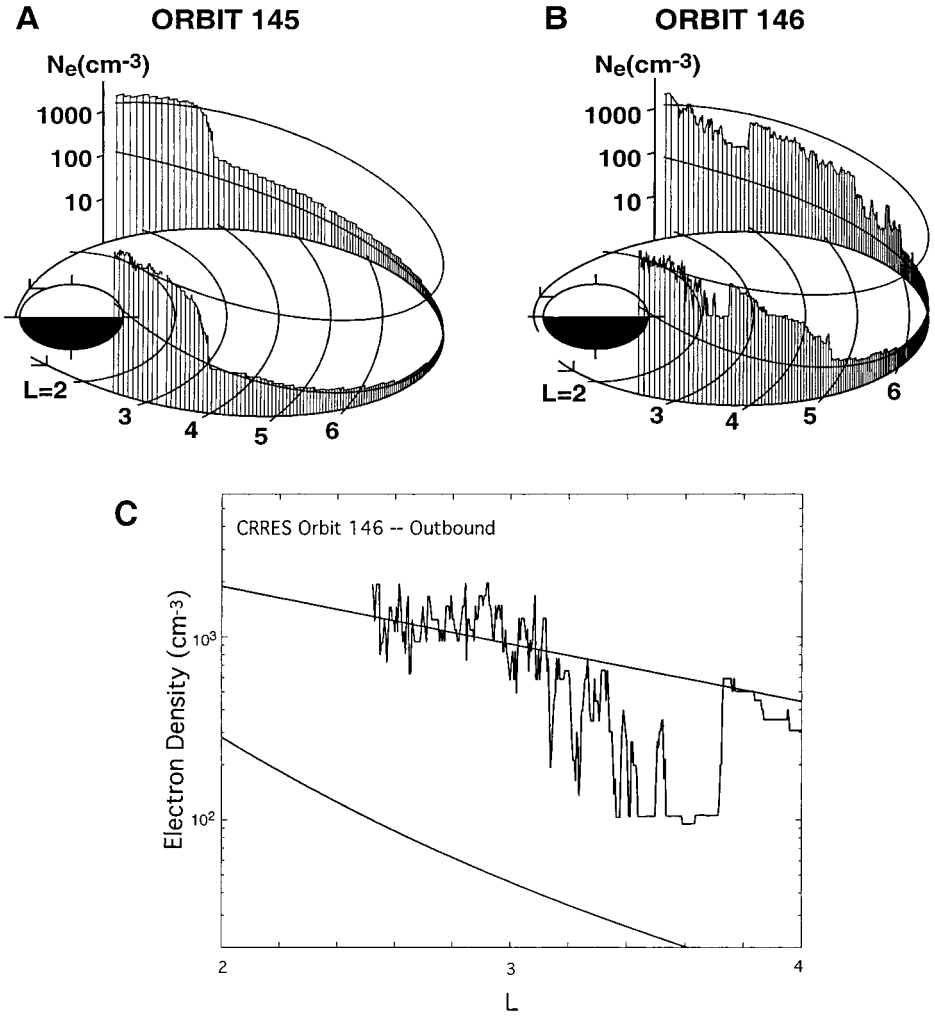

Figure 6. Successive CRRES orbits (145 and 146) showing drastically different plasmapause extents and plasmaspheric density structures (vertical lines indicate the electron density N_e on a logarithmic scale measured along the CRRES orbits). The lower panel (part C) shows a detailed plot of the L-profile of the electrons density observed during the outbound portion of the CRRES orbit 146 (adapted from Carpenter et al., 1999).

The frequency ranges required for RPI sounding of the plasmasphere are commensurate with the expected plasma frequencies (see right scale of Figure 5) and the R-X cutoff [(2)]. For densities in the region of plasmapause and beyond, the appropriate frequency range is approximately 10–200 kHz. Fixed or selected frequencies in the range ~80–100 kHz may be useful for efficient probing of a steep plasmapause on some occasions. For probing the interior profile of the plasmasphere from within the plasmatrough region (e.g., at L > 4 in Figure 6A),

frequencies in the range ∼100−500 kHz will be needed. For sounding from relatively low altitudes within the plasmasphere, the range 100 kHz−3 MHz will be needed, this being a form of 'topside sounding.'

In order to capture the dynamical variations, one would like to detect changes in the equatorial radius of the plasmapause at speeds ranging from 0 to 200 km per minute. While these velocities are small compared to magnetopause motions, they need to be considered by accounting for the spacecraft velocity at various points along the IMAGE orbit [see (7)−(9a)]. Range resolution is another important limiting factor in study of the plasmasphere shape and dynamics. Note that some of the best opportunities for studying the plasmapause profile and its dynamics will come when IMAGE is relatively close to the plasmapause, but that the shortest possible pulse and dead time may be needed under those circumstances.

Small-scale density fluctuations have been observed by the CRRES satellite near the plasmapause (LeDocq et al., 1994). On many occasions when the CRRES apogee was near the plasmapause and the spacecraft was moving eastward more or less at constant geocentric distance, individual irregularities appeared, each surrounded on the record by plasmatrough level densities. An example can be seen in the data for Figure 6B (Carpenter et al., 1999). Some of these irregularities may have a width of the order of a few hundred km, and may even have finer structure as shown in a detailed plot of the L-profile of the electron densities observed during outbound portion of the CRRES orbit 146 (Figure 6(C)).

The RPI can also be programmed (Reinisch et al., 2000) to perform relaxation sounding by concentrating on short-range plasma resonances. In this case, it is possible to rapidly sweep over a selected frequency interval. Such a relaxation sounding program can be interspersed among normal long-range soundings. With a 300-Hz RPI receiver bandwidth, the density resolution is expected to be a few percent. There will be a great variety of irregular structures formed at and near the plasmapause as illustrated in Figures 5 and 6. At times the plasmapause scale width may be less than 100 km near the equator, and less than 10 km at ionospheric heights. For these cases, it may be fruitful to combine relaxation sounding observations of irregularities and of the plasmapause with local measurements of density and possibly electron temperature by quasi-thermal noise observations (Reinisch et al., 2000; Green et al., 2000; Meyer-Vernet, 1998).

Measurements of rapidly changing quantities may best be made by some combination of passive recording and relaxation sounding or antenna impedance measurements in the whistler-mode frequency range. In the cases of passive recording and relaxation sounding, changes in plasma parameters with time would be deduced from the corresponding changes in resonance frequencies in the plasma, such as at the plasma or upper hybrid frequencies.

It is of interest to consider the information expected to be obtained by the RPI along an IMAGE orbit (Fuselier et al., 2000). Figure 7 shows the IMAGE orbital configuration during the early phase of the mission. On a given upleg (C, D), RPI is located outside the plasmasphere and should obtain some information on the global

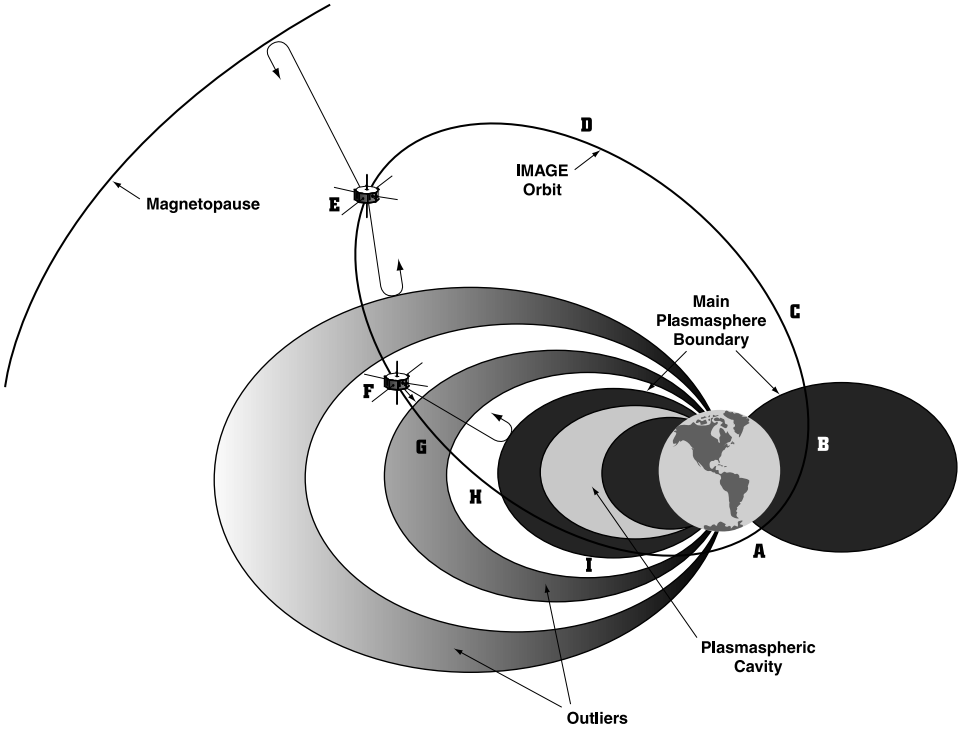

Figure 7. Schematic of IMAGE orbital configuration during the early phase of the mission, illustrating favorable positions for RPI observations of the plasmapause and plasmasphere.

average size of the plasmasphere. For an extended range of spacecraft positions between location C and D, for example, reflections from the plasmapause should arrive from a distorted ring in local time around the magnetic pole. In addition, differences in range of echoes arriving from various bearings may provide information on the large variations in plasmapause L value with longitude, thus revealing any asymmetry imposed upon the plasmasphere by spatially and temporally irregular processes that act upon it. On the downleg (E, F, G, H), RPI is inside the plasmasphere and should be able to obtain detailed information on the L value and variation in L value with local time (compared to the upleg measurements) of the plasmapause over a several-hour period. It should be able to measure the density profile between IMAGE and points well within the plasmasphere, and detect important changes in that profile with time, such as the appearance of irregularities, refilling of depleted regions, loss of plasma from particular regions, and changes in density gradient. With apogee in the afternoon sector, the early phase of IMAGE will offer the best chance to study outlying dense regions, as indicated in Figures 5 and 6 and discussed in Green et al. (2000).

The outliers shown in Figure 5 will not necessarily lie in the plane of the IMAGE orbit. Some of these outlying plasma structures may be tail-like and connected to the main plasmasphere, while others may be more or less detached from that body. RPI should have a unique opportunity to investigate these poorly known forms. Discussion of expected RPI observations to investigate the newly discovered plasmaspheric cavity, a density depleted region within the plasmsphere as indicated in Figure 6, has been given by Green et al. (2000).

When IMAGE is at relatively low altitude within the plasmasphere and in the southern polar region (I,A,B), it should be able to sound the topside ionosphere and thus determine the low-altitude conditions associated with the observations made at higher altitude on the opposite pole of the Earth. Such comparison of the high- and low-altitude observations between opposite poles can provide information on plasma boundary conditions on conjugate points along a given geomagnetic flux tube as a function of local time.

4.2. MAGNETOPAUSE AND BOUNDARY LAYER

The global magnetopause configuration changes in response to the variations in solar wind pressure and interplanetary magnetic field orientation. In addition, it is expected that large-scale surface waves (see, e.g., Haerendel et al., 1978; Hones et al., 1981; Anderson et al., 1982; Song et al., 1988; Ogilvie and Fitzenreiter, 1989; Fairfield, 1991; Sibeck et al., 1991; Petrinec and Russell, 1993; Roelof and Sibeck, 1993, 1994) and small-scale irregularities (Anderson et al., 1982; Gary and Sgro, 1990; Drake et al., 1994) are usually present in the magnetopause and its boundary layers. Such global and local variations tend to complicate the analysis and interpretation of *in situ* measurements obtained near the magnetopause region (Sckopke et al., 1981; Elphic, 1990; Sibeck and Smith, 1992; Song et al., 1994). In the presence of surface irregularities, for example, single spacecraft measurements are subject to temporal and spatial aliasing, making the determination of plasma or magnetic boundary crossings difficult. Correlated, high-resolution plasma and magnetic field measurements from multiple spacecraft are therefore needed to discern the various spatial and temporal scales present in the magnetopause and boundary layer region.

Information on plasma irregularities in the magnetopause boundary layer can also be deduced from observations by the RPI on IMAGE. If the irregularity scale lengths are larger than the Fresnel zone, the reflecting surface will be coherent and will specularly reflect the sounder signals (provided $r < r_c$, see (17)). The different phases of a surface wave in the magnetospheric boundary layer will produce multiple echoes (as illustrated in Figure 8). The orientation of the density surfaces, given by the echo ray directions, can then be used to reconstruct the surface wave, yielding scale size information. Moreover, if the propagation time of the surface wave (transit time of one wavelength) is longer than the echo delay time, it will then be possible to use a magnetospheric sounder to monitor the motion

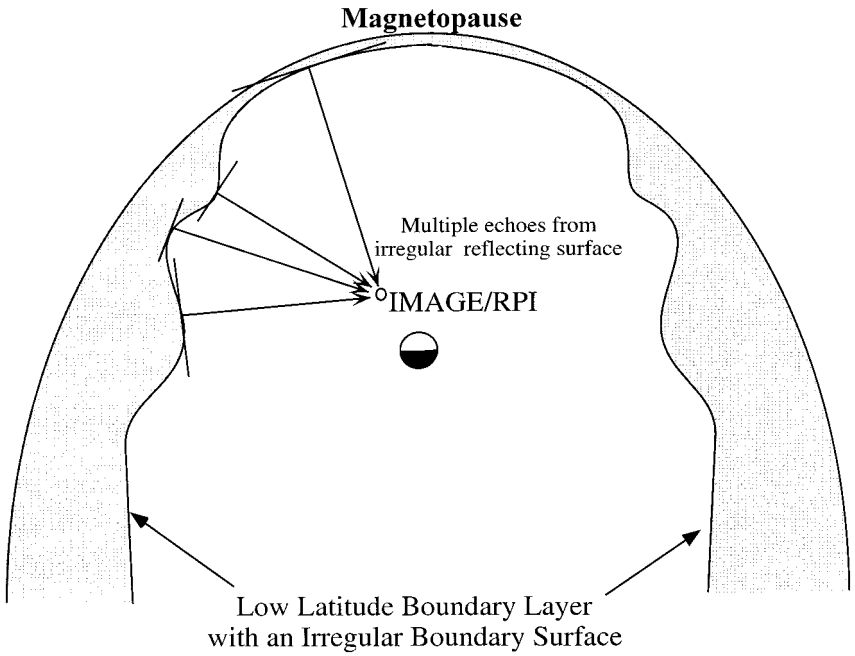

Figure 8. A sketch of multiple echoes being returned by the different phases of a surface wave in the boundary layer and detected by the sounder.

of the irregularity, discerning boundary motions from surface wave propagation. Therefore, the radio sounding technique promises to be as successful in probing magnetospheric boundary and plasma regimes as it has been in the ionosphere.

5. Discussion and Conclusions

The varying positions of IMAGE along its orbit affects primarily the ranges and viewing geometry of various target plasmas, although spacecraft motion along its orbit also contributes to Doppler shifts (Reinisch et al., 1999). Range variations can change the effective Fresnel radii R_F (Equation (5)) for echoes arriving from different directions. With fluctuations (Δr, $\Delta \mathbf{k}$) introduced by plasma irregularities in remote plasma target regions, we expect the coherence or degree of polarization of an echo at a fixed frequency to vary with IMAGE position as $\mathbf{r}$ varies. These effects may be observable in both magnetopause (boundary layer) and plasmapause (plasmasphere) echoes at different frequencies, particularly during periods of increased noise level. Unlike *in situ* measurements of magnetospheric plasmas, which cannot always distinguish between spatial and temporal variations, high-time resolution observations by the RPI will yield spatial structure of magnetospheric plasmas.

Like the ionosphere, plasma irregularities with different scale sizes are expected to be present in magnetospheric plasmas. Irregularity scale sizes (λ_i) can vary

from much larger to much smaller than the wavelengths (λ) of the sounder waves. When the intervening plasma irregularities or turbulence has $\lambda_{De} < \lambda_i < \lambda$, the sounder waves can be coherently scattered to produced spread echoes in both frequency and range, analogous to the spread F signature in the ionospheric case (see Subsection 3.1). Such scattering can effectively reduce the power of a primary echo and increase the chances of secondary echoes, as discussed in Section 2.3. In order for the RPI to receive a strong primary echo, it is necessary that only very weak turbulence is present at $\lambda_i < \lambda$ in the plasma medium between the RPI (IMAGE) and the target plasma. Since the effects of incoherent scattering, which occurs when $\lambda_{De} > \lambda$, are likely to be negligible in the RPI measurements, we have neglected the echo power losses due to this process in this discussion. Longer wavelength irregularities (at $\lambda_i \gg \lambda$) will also scatter the sounder waves. Such scattering, however, will not likely alter significantly the propagation direction of the sounder wave (see (18)). From these considerations, it is expected that the echo characteristics measured by the RPI can be quite complex, depending on the nature (fluctuating frequencies, scale sizes and amplitudes) of the irregularities present in the intervening and target plasmas. These effects need to be accounted for when analyzing RPI data. Coherent integration techniques are applicable only when the target range r is less than r_c (17) which can be quite readily satisfied for both ionospheric and magnetospheric sounding.

RPI has the ability to make Doppler and spectral measurements, and thus the echo characteristics for each Doppler/spectral component can be analyzed separately. Consistent and repetitive measurements of the magnetopause/boundary layer and plasmaspheric echoes at different RPI positions along the IMAGE orbit (with varying R_F) will yield information on the characteristic scale sizes of the irregularities present in these regions. Determination of characteristic irregularity length scales can lead to the identification of their generation mechanisms and understanding of the associated plasma dynamics.

Acknowledgements

The authors would like to express their gratitude for stimulating discussions and comments on the manuscript of this paper from J. L. Green, P. H. Reiff, and W. W. L. Taylor.

References

Anderson, R. R., Harvey, C. C., Hoppe, M. M., Tsurutani, B. T., Eastman, T. E. and Etcheto, J.: 1982, 'Plasma Waves Near the Magnetopause', *J. Geophys. Res.* **87**, 2087.

Ahkiezer, A. I., Akhiezer, I. A., Polovin, R. V., Sitenko, A. G. and Stepanov, K. N.: 1975, *Plasma Electrodynamics 1&2*, Pergamon Press, Oxford.

Benson, R. F., Green, J. L., Fung, S. F., Reinisch, B. W., Calvert, W., Haines, D. M., Bougeret, J.-L., Manning, R., Carpenter, D. L., Gallagher, D. L., Reiff, P. H. and Taylor, W. W. L.: 1998, 'Magnetospheric Radio Sounding on the IMAGE Mission', *Radio Sci. Bull*. **285**, 9–20; also available from: http://image.gsfc.nasa.gov/.

Bibl, K. and Reinisch, B. W.: 1978, 'The Universal Digital Ionosonde', *Radio Sci.*, **13**, 519.

Budden, K. G.: 1985, *The Propagation of Radio Waves*, Cambridge University Press, Cambridge.

Calvert, W.: 1995, 'Wave Ducting in Different Wave Modes', *J. Geophys. Res.* **100**, 17,491.

Calvert, W., Benson, R. F., Carpenter, D. L., Fung, S. F., Gallagher, D. L., Green, J. L., Haines, D. M., Reiff, P. H., Reinisch, B. W., Smith, M. F. and Taylor, W. W. L.: 1995, 'The Feasibility of Radio Sounding in the Magnetosphere', *Radio Sci.* **30**, 1577.

Calvert, W., Benson, R. F., Carpenter, D. L., Fung, S. F., Gallagher, D. L., Green, J. L., D. M Haines, D. M., Reiff, P. H., Reinisch, B. W., Smith, M. F. and Taylor, W. W. L.: 1997, 'Reply to Comment on "The Feasibility of Radio Sounding in the Magnetosphere"', *Radio Sci.* **32** (1), 281.

Carpenter, D. L. and Anderson, R. R.: 1992, 'An ISEE/Whistler Model of Equatorial Electron Density in the Magnetosphere', *J. Geophys. Res.* **97**, 1097.

Carpenter, D. L. and Lemaire, J.: 1997, 'Erosion and Recovery of the Plasmasphere in the Plasmapause Region', *Space Sci. Rev.* **80**, 153.

Carpenter, D. L., Anderson, R. R., Calvert, W. and Moldwin, M. B.: 1999, 'CRRES Observations of Density Cavities within the Plasmasphere', unpublished manuscript.

Carpenter, D. L., Giles, B. L., Chappell, C. R., Decreau, P. M. E., Anderson, R. R., Persoon, A. M., Smith, A. J., Corcuff, Y. and Canu, P.: 1993, 'Plasmasphere Dynamics in the Duskside Bulge Region: a New Look at an Old Topic', *J. Geophys. Res*. **98**, 19243.

Davidson, R. C.: 1972, *Methods in Nonlinear Plasma Theory*, Academic Press, New York.

Drake, J. F., Gerber, J. and Kleva, R. G.: 1994, 'Turbulence and Transport in the Magnetopause Current Layer', *J. Geophys. Res*. **99**, 11211.

Dyson, P. L. and Benson, R. F.: 1978, 'Topside Sounder Observations of Equatorial Bubbles', *Geophys. Res. Lett*. **5**, 795.

Elphic, R. C.: 1990, 'Observations of Flux Transfer Events: are FTEs Flux Ropes, Islands, or Surface Waves?', in: C. T. Russel, E. R. Priest, and L. C. Lee (eds), *Physics of Magnetic Flux Ropes*, *Geophys. Monogr.* **58**, AGU, Washington, D.C., 455–471.

Fairfield, D. H.: 1991, 'Solar Wind Control of the Size and Shape of the Magnetosphere', *J. Geomag. Geoelect. Suppl.* **43**, 117.

Fejer, B. G. and Kelley, M. C.: 1980, 'Ionospheric irregularities,' *Rev. Geophys. Space Phys*. **18**, 401.

Flock, W. L.: 1979, *Electromagnetics and the Environment: Remote Sensing and Telecommunications*, Prentice-Hall, Inc., Englewood Cliffs, New Jersey.

Franklin, C. A. and Maclean, M. A.: 1969, 'The Design of Swept-Frequency Topside Sounders', *Proc. IEEE* **57**, 897.

Fung, S. F. and Green, J. L.: 1996, 'Global Imaging and Remote Sensing of the Magnetosphere,' in *Radiation Belts: Models and Standards*, Geophysical Monographs **97**, American Geophysical Union, Washington, D.C., 285–290.

Fuselier, S. A., Burch, J. L., Lewis, W. and Reiff, P. H.: 2000, 'Overview of the IMAGE Science Objectives and Mission Phases', *Space Sci. Rev.* **91**, 51–66 (this issue).

Gary, S. P. and Sgro, A. G.: 1990, 'The Lower Hybrid Drift Instability at the Magnetopause', *Geophys. Res. Lett.*, **17**, 909.

Green, J. L., Benson, R. F., Fung, S. F., Taylor, W. W. L., Boardsen, S. A., Reinisch, B. W., Haines, D. M., Bibl, K., Cheney, G., Galkin , I. A., Huang, X., Meyers, S. H., Sales, G. S., Bougeret, J.-L., Manning, R., Meyer-Vernet, N., Moncuquet, M., Carpenter, D. L., Gallagher, D. L. and Reiff, P. H.: May 2000, 'Radio Plasma Imager Simulations and Measurements', *Space Sci. Rev.* **91**, 361–389 (this issue).

Green, J. L., Taylor, W. W. L., Fung, S. F., Benson, R. F., Calvert, W., Reinisch, B. W Gallagher, D. L. and Reiff, P. H.: 1998, 'Radio Remote Sensing of Magnetospheric Plasmas', in *Measurement Techniques in Space Plasma: Fields*, Geophys. Monogr., 103, AGU, Washington, D. C., pp. 193 –198.

Hecht, E. and Zajac, A.: 1976, *Optics*, Addison-Wesley Pub. Co., Reading, MA.

Haerendel, G., Paschmann, G., Sckopke, N., Rosenbauer, H. and Hedgecook, P. C.: 1978, 'The Frontside Boundary Layer and the Problem of Reconnection', *J. Geophys. Res*. **83**, 3195.

Hagg, E. L., Hewensand, E. J., Nelms and G. L.: 1969, 'The Interpretation of Topside Sounder Ionograms', *Proc. IEEE* **57**, 949.

Haines, D. M.: 1994, 'A Portable Ionosonde Using Coherent Spread-Spectrum Waveforms for Remote Sensing of the Ionosphere', Ph.D. Dissertation, Department of Electrical Engineering, University of Massachusetts, Lowell.

Hanuise, C.: 1983, 'High-Latitude Ionospheric Irregularities: a Review of Recent Radar Results', *Radio Sci.* **18**, 1093.

Hargreaves, J. K.: 1992, *The Solar-Terrestrial Environment*, Cambridge University Press, Cambridge.

Hones, E. W., Jr., Birn, J., Bame, S. J., Asbridge, J. R., Paschmann, G., Sckopke, N. and Haerendel, G.: 1981, 'Further Determination of the Characteristics of Magnetospheric Plasma Vortices with ISEE 1 and 2', *J. Geophys. Res.* **86**, 814.

Horwitz, J. L., Comfort, R. H. and Chappell, C. R.: 1990, 'A Statistical Characterization of Plasmasphere Density Structure and Boundary Locations', *J. Geophys. Res.* **95**, 7937.

Huang, X. and Reinisch, B. W.: 1982, 'Automatic Calculation of Electron Density Profiles from Digital Ionograms. 2. True Height Inversion of Topside Ionograms with the Profile-Fitting Method', *Radio Sci.* **17** (4), 837.

Hunsucker, R. D.: 1992, *Radio Techniques for Probing the Terrestrial Ionosphere*, Vol. 22, Phys. Chem. Space, Springer-Verlag, Berlin.

Jackson, J. E.: 1969, 'The Reduction of Topside Ionograms to Electron-Density Profiles', *Proc. IEEE* **57**, 960.

Jackson, J. E., Schmerling, E. R. and Whitteker, J. H.: 1980, 'Mini-Review on Topside Sounding', *IEEE Trans. Antennas Propagat*. **AP-28**, 284.

James, H. G.: 1989, 'ISIS 1 Measurements of High-Frequency Backscatter Inside the Ionosphere', *J. Geophys. Res.* **94**, 2617.

Jelly, D. H. and Petrie, L. E.: 1969, 'The High-Latitude Ionosphere', *Proc. IEEE* **57**, 1005.

Kelly, M. C.: 1989, *The Earth's Ionosphere*, Academic Press, Inc., San Diego, CA.

Keskinen, M. J. and Ossakow, S. L.: 1983, 'Theories of High-Latitude Ionospheric Irregularities: a Review', *Radio Sci*. **18**, 1077.

Koons, H. C.: 1989, 'Observations of Larger-Amplitude, Whistler Mode Wave Ducts in the Outer Plasmasphere', *J. Geophys. Res.* **94**, 15383.

Kruer, W. L.: 1988, *The Physics of Laser Plasma Interactions*, *Frontiers in Physics Lecture Note Series*, Addison-Wesley Publishing Co., Inc.

Lemaire, J. L. and Gringauz, K. I.: 1998, *The Earth's Plasmasphere*, Cambridge University Press, Cambridge.

LeDocq, M. J., Gurnett, D. A. and Anderson, R. R.: 1994, 'Electron Number Density Fluctuations near the Plasmapause Observed by the CRRES Spacecraft', *J. Geophys. Res.* **99**, 23661.

Meyer-Vernet, N., Hoang, S., Issautier, K., Maksimovic, M., Manning, R., Moncuquet, M. and Stone, R.: 1998, 'Measuring Plasma Parameters with Thermal Noise Spectroscopy', in E. Borovsky and

R. Pfaff (eds), Geophysical Monograph 103: *Measurements techniques in Space Plasmas*, AGU, Washington, D. C., pp. 205–210.

Moldwin, M. B., Thomsen, M. F., Bame, S. J., McComas, D. and Reeves, G. D.: 1995, 'The Fine-Scale Structure of the Outer Plasmasphere', *J. Geophys. Res.* **100**, 9649.

Muldrew, D. B.: 1969, 'Nonvertical Propagation and Delayed-Echo Generation Observed by the Topside Sounders', *Proc. IEEE* **57**, 1097.

Ogilvie, K. W. and Fitzenreiter, R. J.: 1989, 'The Kelvin-Helmholtz Instability at the Magnetopause and Inner Boundary Layer Surface', *J. Geophys. Res.* **94**, 15113.

Oya, H. and Ono, T.: 1987, 'Stimulation of Plasma Waves in the Magnetosphere Using Satellite JIKIKEN (EXOS B) Part II: Plasma Density Across the Plasmapause', *J. Geomag. Geoelectr.* **39**, 591.

Petrinec, S. M. and Russell, C. T.: 1993, 'External and Internal Influences on the Size of the Dayside Terrestrial Magnetosphere', *Geophys. Res. Lett.* **20**, 339.

Pulinets, S. A. and Selegey, V. V.: 1986, 'Ionospheric Plasma Modification in the Vicinity of a Spacecraft by Powerful Radio Pulses in Topside Sounding', *J. Atm. and Terr. Phys.* **48**, 149.

Ratcliffe, J. A.: 1970, *Sun, Earth and Radio: An Introduction to the Ionosphere and Magnetosphere*, McGraw-Hill Book Company, New York, 256 pp.

Ratcliffe, J. A.: 1972, *An Introduction to the Ionosphere and Magnetosphere*, Cambridge University Press, London, 256 pp.

Reiff, P. H., Boyle, C. B., Green, J. L., Fung, S. F., Benson, R., Calvert, W. and Taylor, W. W. L.: 1996, 'Radio Sounding of Multi-Scale Plasmas', in T. Chang and J. R. Jasperse (eds), *Physics of Space Plasmas*, **14**, MIT Press, Cambridge, MA, pp. 415–429.

Reinisch, B. W.: 1996, 'Modern Ionosondes', in H. Kohl, R. Rüster and K. Schlegel (eds), *Modern Ionospheric Science*, *European Geophysical Society*, 37191 Katlenburg-Lindau, ProduServ GmbH Verlagsserie, Berlin, Germany, pp. 440–458.

Reinisch, B. W., Bullett, T. W., Scali, J. L. and Haines, D. M.: 1995, 'High Latitude Digisonde Measurements and their Relevance to IRI', *Adv. Space Res.* **16** (1), 17.

Reinisch, B. W., Haines, D. M., Bibl, K., Cheney, G., Galkan, I. A., Huang, X., Myers, S. H., Sales, G. S., Benson, R. F., Fung, S. F., Green, J. L., Taylor, W. W. L., Bougeret, J.-L., Manning, R., Meyer-Vernet, N., Moncuquet, M., Carpenter, D. L., Gallagher, D. L. and Reiff, P. H.: 2000, 'The Radio Plasma Imager Investigation on the IMAGE Spacecraft', *Space Sci. Rev.* **91**, 315–359 (this issue).

Reinisch, B. W., Sales, G. S., Haines, D. M., Fung, S. F. and Taylor, W. W. L.: 1999, 'Radio Wave Active Doppler Imaging of Space Plasma Structures: Angle-of-Arrival, Wave Polarization, and Faraday Rotation Measurements with RPI', *Radio Sci.* (in press).

Roelof, E. C. and Sibeck, D. G.: 1993, 'Magnetopause Shape as a Bivariate Function of Interplanetary Magnetic Field Bz and Solar Wind Dynamic Pressure', *J. Geophys. Res.* **98**, 21421.

Roelof, E. C. and Sibeck, D. G., 1994, 'Correction to Magnetopause Shape as a Bivariate Function of Interplanetary Magnetic Field Bz and Solar Wind Dynamic Pressure', *J. Geophys. Res.* **99**, 8787.

Sales, G. S., Reinisch, B. W., Scali, J. L., Dozois, C., Bullett, T. W., Weber, E. J. and Ning, P.: 1996, 'Spread F and the Structure of Equatorial Ionization Depletions in the Southern Anomaly Region', *J. Geophys. Res.* **101**, 26819.

Sckopke, N., Paschmann, G., Haerendel, G., Sonnerup, B. U. Ö., Bame, S. J., Forbes, T. G., Hones, E. W. and Russell, C. T.: 1981, 'Structure of the Low Latitude Boundary Layer', *J. Geophys. Res.* **86**, 2099.

Sibeck, D. G. and Smith, M. F.: 1992, 'Magnetospheric Plasma Flows Associated with Boundary Waves and Flux Tansfer Events', *Geophys. Res. Lett.* **19**, 1903.

Sibeck, D. G., Lopez, R. E. and Roelof, E. C.: 1991, 'Solar Wind Control of the Magnetopause Shape, Location and Motion', *J. Geophys. Res.* **96**, 5489.

Song, P., Elphic, R. C. and Russell, C. T.: 1988, 'ISEE 1 & 2 Observations of the Oscillating Magnetopause', *Geophys. Res. Lett.* **15**, 744.

Song, P., Le, G. and Russell, C. T.: 1994, 'Observational Differences Between Flux Transfer Events and Surface Waves at the Magnetopause', *J. Geophys. Res.* **99**, 2309.

Stix, T. H.: 1992, *Waves in Plasmas*, AIP Press, New York.

Swanson, D. G.,: 1989, *Plasma Waves*, Academic Press, Inc., San Diego, CA.

Treumann, R. A. and Baumjohann, W.: 1997, *Advanced Space Plasma Physics*, Imperial College Press, London.

Tyler, G. L., Simpson, R. A., Maurer, M. J. and Holmann, E.: 1992, 'Scattering Properties of the Venusian Surface: Preliminary Results from Magellan', *J. Geophys. Res*. **97**, 13115.